Mathematical Biosciences and Engineering

MBE, 18(1): 456–470.
DOI: 10.3934/mbe.2021025
Received: 03 September 2020
Accepted: 02 December 2020
Published: 08 December 2020

http://www.aimspress.com/journal/MBE

Research article

Performance of protein-ligand docking with CDK4/6 inhibitors: a case study

Linlu Song[1], Shangbo Ning[1], Jinxuan Hou[2,*] and Yunjie Zhao[1,*]

[1] Institute of Biophysics and Department of Physics, Central China Normal University, Wuhan 430079, China
[2] Department of Thyroid and Breast Surgery, Zhongnan Hospital of Wuhan University, Wuhan 430071, China

* **Correspondence:** Email: yjzhaowh@mail.ccnu.edu.cn, jhou@whu.edu.cn.

Supplementary

Figure S1. Sequence alignment analysis of the CDK6. The three CDK6 structures extracted from the different experiments have identical sequences. * represents the consensus sequence.

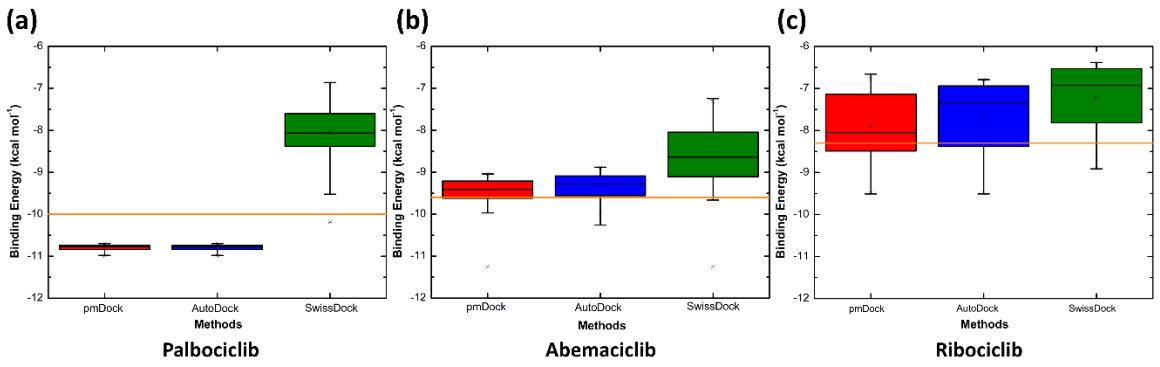

Figure S2. Binding energy analysis of (a) Palbociclib, (b) Abemaciclib, and (c) Ribociclib in top 200 conformations between predicted and experimental results. The orange line is the experimental binding energy. The pmDock shows smaller differences than AutoDock and SwissDock.

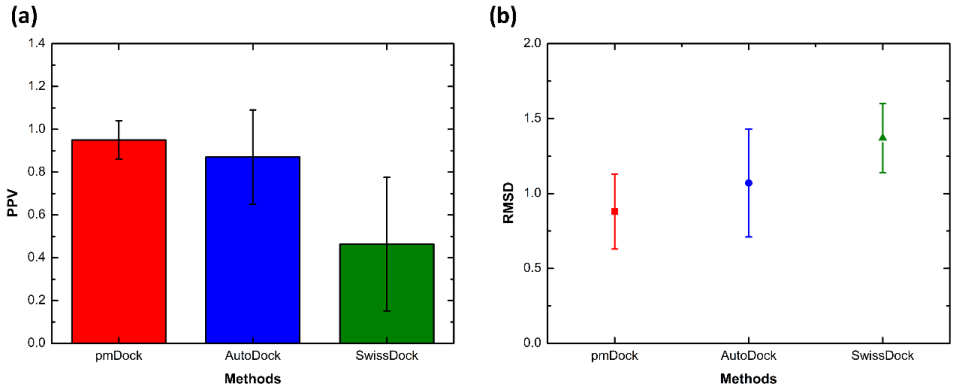

Figure S3. The (a) PPV and (b) RMSD analysis. The red, blue, and green columns are pmDock, AutoDock, and SwissDock, respectively. The calculated the RMSDs of the average conformations of the first clusters in pmDock. The results show pmDock can provide predictions with higher accuracy and smaller RMSD.

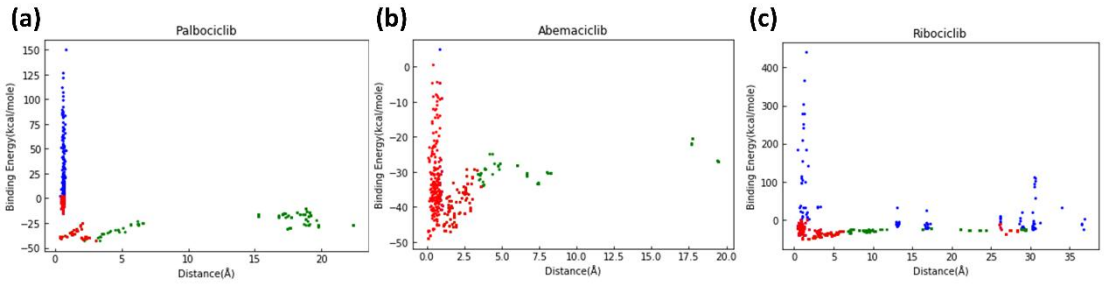

Figure S4. Energy versus distance accuracy plot of the (a) Palbociclib, (b) Abemaciclib, and (c) Ribociclib predictions. The red, blue, and green dots are pmDock, AutoDock, and SwissDock, respectively. The results show pmDock can provide native-like predictions.

Table S1. The list of CDK inhibitors.

Compound	Primary targets	Clinical trials (open, active, or completed)	Ref.
Type I inhibitors			
Roniciclib (BAY1000394)	CDK2 CDK9	Phase II: small cell lung cancer	[1]
CCT251545	CDK8 CDK19	Not yet*	[2]
Dabrafenib (GSK2118436)	CDK16	Phase II: colorectal cancer (CRC), melanoma Phase I: colorectal cancer (CRC)	[3,4]
Type II inhibitors			
Sorafenib	CDK8	Phase III: advanced clear-cell renal-cell carcinoma, hepatocellular carcinoma Phase II: advanced hepatocellular carcinoma	[5]
Rebastinib	CDK16	Phase I: chronic myeloid leukemia	[6]
Type III inhibitors			
NBI1	CDK2	Not yet*	[7,8]

* No clinical trials.

Table S2. The list of docking methods.

Methods	Ref.
Shape Complementary	
Context shapess	[9]
Hex	[10]
ZDOCK&RDOCK	[11]
Monte Carlo	
Affinity	[12]
LigandFit	[13]
Genetic	
AutoDock	[14]
GOLD	[15]
FlexiDock	[16]
GAsDock	[17]

Table S3. The information of CDK6 and inhibitors.

PDB	CDK6 Sequence Length	Inhibitor	Ligand Molecular Formula	Experimental Method	Resolution (Å)
5L2I	307	Palbociclib	$C_{24}H_{29}N_7O_2$	X-ray diffraction	2.75
5L2S	307	Abemaciclib	$C_{27}H_{32}F_2N_8$	X-ray diffraction	2.27
5L2T	307	Ribociclib	$C_{23}H_{30}N_8O$	X-ray diffraction	2.37

Table S4. The average distance between the geometric center of the ligands and the experiments.

Inhibitor	pmDock (Å)	AutoDock (Å)	SwissDock (Å)
Palbociclib	0.77	0.59	13.14
Abemaciclib	1.05	0.58	4.32
Ribociclib	4.63	10.40	13.06
Average	2.15 ± 2.15	3.86 ± 5.67	10.17 ± 5.07

Table S5. Binding site prediction accuracy.

A. Analysis of the predicted binding sites of the top 200 conformations by AutoDock.

Inhibitor	Number of binding sites							Accuracy
	(6	5	4	3	2	1	0)*	
Palbociclib	0	153	44	0	0	0	3	0.78
Abemaciclib	89	110	1	0	0	0	0	0.91
Ribociclib	--	43	55	24	0	13	65	0.52

* 6, 5, 4, 3, 2, 1, 0 represent the number of the binding site (n).

B. Analysis of the predicted binding sites of the top 200 conformations by SwissDock.

Inhibitor	Number of binding sites							Accuracy
	(6	5	4	3	2	1	0)*	
Palbociclib	5	2	23	22	14	85	49	0.26
Abemaciclib	2	34	48	72	8	19	17	0.52
Ribociclib	--	0	7	19	28	48	98	0.19

* 6, 5, 4, 3, 2, 1, 0 represent the number of the binding site (n).

C. Analysis of the predicted binding sites of the conformations by pmDock.

Inhibitor	Number of binding sites							Accuracy
	(6	5	4	3	2	1	0)*	
Palbociclib	5	157	61	11	6	0	0	0.77
Abemaciclib	91	144	46	33	8	1	0	0.81
Ribociclib	--	44	63	43	24	8	22	0.64

* 6, 5, 4, 3, 2, 1, 0 represent the number of the binding site (n).

D. The binding site prediction accuracy of the three methods.

Inhibitor	pmDock	AutoDock	SwissDock
Palbociclib	0.77	0.78	0.26
Abemaciclib	0.81	0.91	0.52
Ribociclib	0.64	0.52	0.19
Average	0.74 ± 0.09	0.74 ± 0.20	0.32 ± 0.17

Table S6. The average binding energy difference between the predictions and the experiments.

Inhibitor	Average binding energy difference (kcal $mole^{-1}$)		
	pmDock	AutoDock	SwissDock
Palbociclib	0.91	0.79	1.96
Abemaciclib	0.61	0.33	1.11
Ribociclib	0.73	0.86	1.17
Average	0.75 ± 0.15	0.66 ± 0.29	1.41 ± 0.47

Table S7. The conservation analysis of the CDK6 structure (PDB code: 5L2S). The evolutionary conservation scores are identified using the ConSurf-DB. The continuous conservation scores are divided into a discrete scale of 9 grades. Grade 1 indicates the most variable positions. Grade 9 shows the most conserved positions.

Conservation	Residues
1–3	LEU6(1), VAL16(1), ARG31(1), LYS34(1), PHE39(1), GLN48(1), SER86(1), ARG87(1), THR88(1), ASP89(1), VAL112(1), PRO113(1), PRO115(1), GLY116(1), GLU120(1), ASP124(1), ASP134(1), GLN158(1), SER171(1), PHE172(1), GLN173(1), ALA175(1), SER195(1), GLY229(1), ASP242(1), ARG245(1), ALA253(1), SER256(1), LYS257(1), SER258(1), ALA259(1), GLU263(1), SER296(1), HIS303(1), LEU33(2), GLY36(2), HIS67(2), PHE80(2), GLU91(2), THR92(2), ILE169(2), TYR170(2), MET174(2), THR198(2), ARG220(2), VAL225(2), ARG251(2), PHE254(2), PRO261(2), PHE265(2), THR267(2), ASP268(2), GLU271(2), LEU272(2), LYS274(2), THR282(2), ALA286(2), TYR292(2), HIS307(2), MET1(3), GLU2(3), GLN11(3), CYS15(3), ALA17(3), GLU18(3), LYS26(3), GLY37(3), ARG38(3), THR49(3), GLY50(3), MET54(3), PRO55(3), LEU56(3), ILE59(3), ALA63(3), THR84(3), ASP110(3), LYS111(3), GLU114(3), PRO118(3), PHE127(3), SER155(3), SER156(3), SER194(3), VAL234(3), GLY239(3), GLU240(3), VAL247(3), HIS255(3), GLN260(3), LYS264(3), LEU278(3), PRO298(3)
4–6	ASP10(4), GLU14(4), ARG46(4), GLU51(4), GLU52(4), GLY53(4), GLU69(4), ARG78(4), VAL85(4), ARG90(4), LYS93(4), ASP102(4), THR106(4), TYR108(4), THR121(4), ARG131(4), SER138(4), HIS139(4), ARG140(4), VAL179(4), LEU192(4), GLN193(4), LYS216(4), SER222(4), LEU232(4), ASP233(4), ILE235(4), GLU241(4), TRP243(4), PRO244(4), ASP246(4), ALA248(4), LEU249(4), PRO250(4), GLN252(4), VAL266(4), ILE269(4), PHE283(4), LYS287(4), GLN301(4), HIS302(4), CYS7(5), ARG8(5), ALA9(5), GLN12(5), GLU21(5), PHE28(5), ASP32(5), VAL47(5), ARG66(5), PRO74(5), VAL82(5), CYS83(5), LEU94(5), THR95(5), HIS100(5), THR107(5), MET126(5), THR154(5), GLY157(5), THR177(5), TRP184(5), PHE209(5), PHE213(5), PRO217(5), ASP224(5), LYS230(5), LEU237(5), ILE262(5), ASP270(5), LEU277(5), LYS279(5), ILE289(5), TYR299(5), ALA23(6), LYS29(6), ASN35(6), ARG44(6), VAL45(6), SER57(6), THR58(6), ARG60(6), VAL64(6), LEU68(6), PHE71(6), GLU72(6), ASP81(6), GLN103(6), LEU109(6), VAL117(6), ILE122(6), LYS123(6), MET125(6), LEU129(6), PHE135(6), VAL153(6), ALA162(6), LEU176(6), SER178(6), LEU183(6), LEU191(6), ALA197(6), PRO199(6), LEU202(6), VAL205(6), ARG214(6), ARG215(6), GLY221(6), SER223(6), ASP226(6), LEU228(6), GLY273(6), CYS280(6), SER293(6), HIS305(6)

Continued on next page

Conservation	Residues
7–9	LYS3(7), ILE19(7), ALA30(7), VAL40(7), LEU42(7), VAL62(7), LEU65(7), THR70(7), VAL76(7), VAL77(7), LEU79(7), LEU96(7), VAL97(7), PHE98(7), VAL101(7), THR119(7), LEU130(7), GLY132(7), LEU133(7), LEU136(7), VAL141(7), VAL142(7), LEU146(7), GLN149(7), ILE151(7), ILE159(7), LEU161(7), LEU166(7), ARG168(7), VAL180(7), VAL190(7), VAL200(7), ILE208(7), ALA210(7), MET212(7), LEU218(7), GLY236(7), ASP275(7), LEU276(7), ASN284(7), SER290(7), LEU295(7), PHE300(7), HIS304(7), ASP4(8), GLY5(8), TYR13(8), TYR24(8), GLY25(8), HIS73(8), ASN75(8), ASP104(8), LEU105(8), GLN128(8), PRO148(8), LEU152(8), LYS160(8), ALA167(8), VAL181(8), ARG186(8), ALA187(8), TYR196(8), CYS207(8), PHE219(8), GLN227(8), ILE231(8), PRO238(8), LEU281(8), PRO285(8), ALA291(8), HIS297(8), HIS306(8), GLY20(9), GLY22(9), VAL27(9), ALA41(9), LYS43(9), GLU61(9), GLU99(9), HIS137(9), HIS143(9), ARG144(9), ASP145(9), LYS147(9), ASN150(9), ASP163(9), PHE164(9), GLY165(9), THR182(9), TYR185(9), PRO188(9), GLU189(9), ASP201(9), TRP203(9), SER204(9), GLY206(9), GLU211(9), ARG288(9), ALA294(9)

Table S8. The critical conserved residue predictions.

A. Analysis of the critical conserved residue predictions by AutoDock.

Inhibitor	Number of correct conformations					Accuracy
	(4	3	2	1	0) *	
Palbociclib	0	156	44	0	0	0.70
Abemaciclib	200	0	0	0	0	1.00
Ribociclib	--	97	25	0	2	0.92

* 4, 3, 2, 1, 0 represent the number of the critical conserved residues (m).

B. Analysis of the critical conserved residue predictions by SwissDock.

Inhibitor	Number of correct conformations					Accuracy
	(4	3	2	1	0) *	
Palbociclib	6	27	16	0	0	0.70
Abemaciclib	56	34	31	12	9	0.70
Ribociclib	--	10	19	1	0	0.77

* 4, 3, 2, 1, 0 represent the number of the critical conserved residues (m).

C. Analysis of the critical conserved residue predictions by pmDock.

Inhibitor	Number of correct conformations					Accuracy
	(4	3	2	1	0) *	
Palbociclib	6	178	56	0	0	0.70
Abemaciclib	254	33	23	12	1	0.91
Ribociclib	--	107	44	1	2	0.89

* 4, 3, 2, 1, 0 represent the number of the critical conserved residues (m).

D. The conserved residues prediction probability in the correct conformations of the three methods.

Inhibitor	pmDock	AutoDock	SwissDock
Palbociclib	0.70	0.70	0.70
Abemaciclib	0.91	1.00	0.70
Ribociclib	0.89	0.92	0.77
Average	0.83 ± 0.12	0.87 ± 0.16	0.72 ± 0.04

Table S9. The critical non-conserved residue predictions.

A. Analysis of the critical non-conserved residue predictions by AutoDock.

Inhibitor	Number of correct conformations			Accuracy
	(2	1	0) *	
Palbociclib	200	0	0	1.00
Abemaciclib	89	110	1	0.72
Ribociclib	45	76	3	0.67

* 2, 1, 0 represent the number of the critical non-conserved residues (m).

B. Analysis of the critical non-conserved residue predictions by SwissDock.

Inhibitor	Number of correct conformations			Accuracy
	(2	1	0) *	
Palbociclib	7	29	13	0.44
Abemaciclib	17	76	49	0.39
Ribociclib	0	19	11	0.32

* 2, 1, 0 represent the number of the critical non-conserved residues (m).

C. Analysis of the critical non-conserved residue predictions by pmDock.

Inhibitor	Number of correct conformations			Accuracy
	(2	1	0) *	
Palbociclib	207	21	12	0.91
Abemaciclib	106	178	39	0.60
Ribociclib	45	95	14	0.60

* 2, 1, 0 represent the number of the critical non-conserved residues (m).

D. The non-conserved residues prediction probability in the correct conformations of the three methods.

Inhibitor	pmDock	AutoDock	SwissDock
Palbociclib	0.91	1.00	0.44
Abemaciclib	0.60	0.72	0.39
Ribociclib	0.60	0.67	0.32
Average	0.70 ± 0.18	0.80 ± 0.18	0.38 ± 0.06

Table S10. The non-CDK targeting compound set.

A. The predicted non-CDK targeting compound information.

ChEMBL No.	Ligand Molecular Formula	Similarity
CHEMBL272332	$C_{25}H_{31}N_7O_2$	0.77
CHEMBL205409	$C_{29}H_{30}FN_7O$	0.41
CHEMBL257665	$C_{26}H_{31}N_7O_2$	0.22

B. The prediction probability of the three methods.

ChEMBL No.	pmDock	AutoDock	SwissDock
CHEMBL272332	1.00	1.00	0.35
CHEMBL205409	0.64	0.33	0.53
CHEMBL257665	1.00	1.00	0.26
Average	0.88 ± 0.21	0.78 ± 0.39	0.38 ± 0.14

References

1. P. Ayaz, D. Andres, D. A. Kwiatkowski, C. C. Kolbe, P. Lienau, G. Siemeister, et al., Conformational adaption may explain the slow dissociation kinetics of roniciclib (BAY 1000394), a type I CDK inhibitor with kinetic selectivity for CDK2 and CDK9, *ACS Chem. Biol.*, (2016), acschembio.6b00074.
2. T. Dale, P. A. Clarke, C. Esdar, D. Waalboer, O. Adeniji-Popoola, M. J. Ortiz-Ruiz, et al., A selective chemical probe for exploring the role of CDK8 and CDK19 in human disease, *Nat. Chem. Biol.*, 2015.
3. M. Schreuer, V. Kruse, Y. Jansen, B. Neyns, COMBI-rechallenge: a phase II clinical trial on dabrafenib plus trametinib in BRAFV600-mutant melanoma patients who previously experienced progression on BRAF(+MEK)-inhibition, *Ann. Oncol.*, **27** (2016).
4. R. B. Corcoran, G. S. Falchook, J. R. Infante, O. Hamid, W. A. Messersmith, E. L. Kwak, et al., BRAF V600 mutant colorectal cancer (CRC) expansion cohort from the phase I/II clinical trial of BRAF inhibitor dabrafenib (GSK2118436) plus MEK inhibitor trametinib (GSK1120212), *J. Clin. Oncol.*, 2012.
5. T. Wang, Z. Yang, Y. Zhang, W. Yan, F. Wang, L. He, et al., Discovery of novel CDK8 inhibitors using multiple crystal structures in docking-based virtual screening, *Eur. J. Med. Chem.*, **129** (2017), 275–286.
6. S. E. Dixon-Clarke, S. N. Shehata, T. Krojer, T. D. Sharpe, F. Von Delft, K. Sakamoto, et al., Structure and inhibitor specificity of the PCTAIRE-family kinase CDK16, *Biochem. J.*, **474** (2017), 699–713.
7. N. Canela, M. Orzaez, R. Fucho, F. Mateo, R. Gutierrez, A. Pineda-Lucena, et al., Identification of an hexapeptide that binds to a surface pocket in cyclin A and inhibits the catalytic activity of the complex cyclin-dependent kinase 2-cyclin A, *J. Biol. Chem.*, **281** (2006), 35942–35953.
8. M. Orzáez, T. Guevara, M. Sancho, E. Pérez-Payá, Intrinsic caspase-8 activation mediates sensitization of erlotinib-resistant tumor cells to erlotinib/cell-cycle inhibitors combination treatment, *Cell Death Dis.*, 2012.
9. Z. Shentu, M. A. Hasan, C. Bystroff, M. J. Zaki, Context shapes: Efficient complementary shape matching for protein-protein docking, *Proteins-Struct. Funct. Bioinformatics*, **70** (2010), 1056–1073.
10. D. W. Ritchie, Evaluation of protein docking predictions using Hex 3.1 in CAPRI rounds 1 and 2, *Proteins: Struct., Funct., Bioinformatics*, 2003.
11. K. Wiehe, B. Pierce, J. Mintseris, W. W. Tong, R. Anderson, R. Chen, et al., ZDOCK and RDOCK performance in CAPRI rounds 3, 4, and 5, *Proteins-Struct. Funct. Bioinformatics*, **60** (2005), 207–213.
12. P. Reigan, W. Guo, D. Siegel, D. Ross, Molecular docking studies investigating the interaction of a series of benzoquinone ansamycin Hsp90 inhibitors with NAD(P)H:quinone oxidoreductase 1 (NQO1), *Cancer Res.*, **66** (2006), 457–457.
13. C. M. Venkatachalam, X. Jiang, T. Oldfield, M. Waldman, LigandFit: a novel method for the shape-directed rapid docking of ligands to protein active sites, *J. Mol. Graphics Model.*, **21** (2003), 289–307.
14. F. Sterberg, G. M. Morris, M. F. Sanner, A. J. Olson, D. S. Goodsell, Automated docking to multiple target structures: Incorporation of protein mobility and structural water heterogeneity in AutoDock, *Proteins-Struct. Funct. Bioinformatics*, **46** (2002), 34–40.

15. G. Jones, P. Willett, R. C. Glen, A. R. Leach, R. Taylor, Development and validation of a genetic algorithm for flexible docking, *J. Mol. Biol*., **267** (1997), 727–748.
16. H. Jing, X. Zhou, X. Dong, J. Cao, H. Zhu, J. Lou, et al., Abrogation of Akt signaling by Isobavachalcone contributes to its anti-proliferative effects towards human cancer cells, *Cancer Lett.*, **294** (2010), 167–177.
17. H. Li, C. Li, C. Gui, X. Luo, K. Chen, J. Shen, et al., GAsDock: a new approach for rapid flexible docking based on an improved multi-population genetic algorithm, *Bioorg. Med. Chem. Lett.*, **14** (2004), 4671–4676.

AIMS Press